Proceeding Paper

Precipitation Time Series Analysis and Forecasting for Italian Regions [†]

Ebrahim Ghaderpour [1,2,*] , **Hanieh Dadkhah** [1] , **Hamed Dabiri** [1,*] , **Francesca Bozzano** [1,2] , **Gabriele Scarascia Mugnozza** [1,2] **and Paolo Mazzanti** [1,2]

1   Department of Earth Sciences & CERI Research Centre, Sapienza University of Rome, 00185 Rome, Italy;
    hanieh.dadkhah@uniroma1.it (H.D.); francesca.bozzano@uniroma1.it (F.B.);
    gabriele.scarasciamugnozza@uniroma1.it (G.S.M.); paolo.mazzanti@uniroma1.it (P.M.)
2   NHAZCA s.r.l., Via Vittorio Bachelet, 12, 00185 Rome, Italy
*   Correspondence: ebrahim.ghaderpour@uniroma1.it (E.G.); hamed.dabiri@uniroma1.it (H.D.)
†   Presented at the 9th International Conference on Time Series and Forecasting, Gran Canaria, Spain,
    12–14 July 2023.

Abstract: In Italy, most of the destructive landslides are triggered by rainfall, particularly in central Italy. Therefore, effective monitoring of rainfall is crucial in hazard management and ecosystem assessment. Global precipitation measurement (GPM) is the next-generation satellite mission, which provides the precipitation measurements worldwide. In this research, we employed the available monthly GPM data to estimate the monthly precipitation for the twenty administrative regions of Italy from June 2000 to June 2021. For each region, we applied the non-parametric Mann–Kendall test and its associated Sen's slope to estimate the precipitation trend for each calendar month. In addition, for each region, we estimated a linear trend and the seasonal cycles of precipitation with the antileakage least-squares spectral analysis (ALLSSA) and showed the annual precipitation variations using box plots. Lastly, we compared machine-learning models based on the auto-regressive moving average for monthly precipitation forecasting and showed that ALLSSA outperformed them. The findings of this research provide a significant insight into processing climate data, both in terms of trend-season estimates and forecasting, and can potentially be used in landslide susceptibility analysis.

Keywords: ALLSSA; ARIMA; GPM; landslides; machine learning; Mann–Kendall; precipitation; remote sensing; time series forecasting; trend analysis

1. Introduction

Precipitation is one of the main components of water cycles, which plays a vital role in maintaining atmospheric balance, growing crops, and providing a fresh water supply. Heavy precipitation can damage crops and cause floods, landslides, soil erosion, etc., while the lack of precipitation can result in drought and forest fires [1–5]. Most parts of central Italy are ranked high or very high for landslide hazards, and most of the reported landslides were triggered by heavy precipitation [6,7]. For instance, a comprehensive description of rainfall-induced landslides in large cities was reported in [8]. Therefore, effective, and continuous monitoring of changes in precipitation is crucial for establishing/improving strategies to mitigate the socioeconomic damages from climate change.

Traditionally, ground precipitation gauges have been used to measure precipitation in high temporal resolution. However, in-situ precipitation gauges are limited in number and cannot sufficiently provide good coverage for all regions, particularly mountainous regions [9]. Recent advances in satellite remote sensing have made it possible to measure global precipitation remotely in a pleasant spatial and temporal resolution.

Global precipitation measurement (GPM) is an advanced satellite mission, which has been providing precipitation measurements since the beginning of the 21st century [10]. The integrated multi-satellite retrieval for GPM (IMERG) is a robust algorithm that considers

all satellite microwave precipitation estimates as well as precipitation gauge measurements to provide reliable monthly precipitation estimates [11,12].

In this research, we analyze the monthly GPM measurements obtained for all twenty regions of Italy. We utilize several time series analysis methods to process these measurements. The main contributions of this research are summarized below.

(1)   For each Italian region, we apply the non-parametric Mann–Kendall (MK) test and Sen's slope estimator to estimate the gradient of the precipitation time series corresponding to each calendar month since 2000.

(2)   For each Italian region, we produce the monthly box plots to better visualize the annual variation of precipitation.

(3)   We apply the antileakage least-squares spectral analysis (ALLSSA) to estimate the season and trend components of the 21-year-long monthly GPM time series for each Italian region.

(4)   We compare the performance of time series forecasting methods on the monthly precipitation time series. These methods are auto-regressive integrated moving average (ARIMA), ARIMA with eXogenous factors (ARIMAX), ARIMAX with seasonal terms (SARIMAX), and ALLSSA.

To the best of the authors' knowledge, this is the first time that such analyses have been performed on the GPM measurements in Italy. The results presented in this paper can be used as a guide for a better understanding of the climate dynamics across Italy and for developing management strategies for landslide hazard management and a sustainable environment.

2. Materials and Methods

2.1. Study Region and Datasets

Italy, a country located in southwest Europe and the middle of the Mediterranean Sea, has 20 administrative regions (see Figure 1). Italy has four climate types: Alpine climate in northern Italy (high-elevation), Apennine climate in northern and central Italy (high-elevation), Peninsular climate in the central part of the peninsula, and Mediterranean climate in southern Italy and Sicily and Sardinia islands. The climate maps of Italy for different months are illustrated in [12].
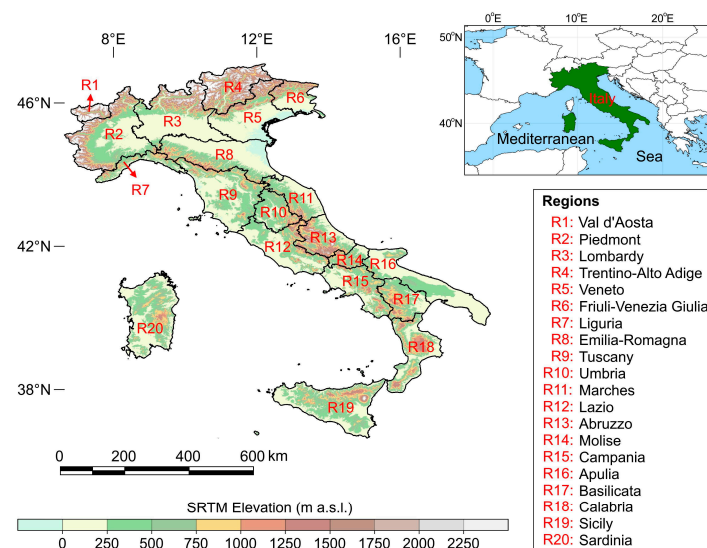

Figure 1. The study area: Italy and its 20 administrative regions. The background elevation in meters above the mean sea level is from the Shuttle Radar Topography Mission (SRTM) plus at ~30 m spatial resolution provided by Jet Propulsion Laboratory (JPL) available freely online at https://doi.org/10.5067/MEaSUREs/SRTM/SRTMGL1N.003 (accessed on 1 January 2023).

The monthly global precipitation measurement (GPM) level 3 data were obtained from all precipitation microwave and infrared satellite estimates and precipitation gauge analyses recommended to use for research [10]. The monthly GPM measurements at a spatial resolution of $0.1° × 0.1°$ were averaged within each Italian region, and their associated standard errors were estimated with the covariance law of error propagation. Therefore, for each Italian region, an unequally weighted time series of size 252 was obtained spanning from June 2000 to June 2021. The weights are inversely proportional to the squares of the measurement errors used in the season-trend estimation with ALLSSA in this study.

2.2. Methods

2.2.1. The Mann–Kendall (MK) Method and Sen's Slope Estimator

The MK method is a non-parametric test for trend analysis widely used in climate studies [13,14]. The null hypothesis in MK is defined as no trend exists in the time series. Thus, if the null hypothesis is rejected, it means there is a statistically significant trend in the time series, the alternative hypothesis. Commonly used confidence levels in the MK test are 90%, 95%, and 99%. The slope of the trends can be obtained via its associated Sen's slope estimator, a non-parametric slope estimator that determines the magnitude and direction of the trend. The mathematical formulas for the MK test and Sen's slope can be found in [13,14]. Herein, to apply the MK test, the monthly precipitation measurements were categorized to obtain a time series of size 21 for each Italian region and each calendar month. Note that the new time series for each calendar month is yearly, i.e., one measurement per year, and so there is no seasonality or intra-annual component in the time series. Then, Sen's slope was estimated for each of the time series of size 21 along with its statistical significance using the MK test.

2.2.2. Boxplots

A boxplot is a graphical representation based on five numbers: the minimum value of the data excluding any outliers, the first quartile Q_1, the median, the third quartile Q_3, and the maximum value of the data excluding any outliers [15]. Values marked as ○ are classified as outliers. An outlier is a value that is either extremely large or extremely small when compared to the rest of the values in a sample. Specifically, an outlier is a value that is larger than the upper fence value or smaller than the lower fence value. These values are calculated as $Q_3 + 1.5(Q_3 − Q1)$ for the upper fence and $Q_1 − 1.5(Q_3 − Q1)$ for the lower fence. Note that the whiskers of the boxplot extend to the most extreme upper and lower points that are not outliers, not to the fence values. Herein, a boxplot for each time series of size 21 mentioned in Section 2.2.1 is also illustrated.

2.2.3. The Antileakage Least-Squares Spectral Analysis (ALLSSA)

ALLSSA is a season-trend fit model based on the least-squares principle [16,17]. In ALLSSA, an initial set of frequencies is first selected along with a type of trend (linear, quadratic, or cubic). Then, an iterative process is performed to simultaneously fit the trend and sinusoids to the time series at a certain confidence level, usually 99%. This process determines an optimal set of sinusoids that, along with the selected trend type, best fit the time series. The algorithm termination is based on the statistical significance of the peaks in the least-squares spectrum, i.e., the process is terminated if there are no more statistically significant spectral peaks in the least-squares spectrum, depending on the initial selected set of frequencies. The code of ALLSSA is described in [15] and is freely available online. ALLSSA can also be used for forecasting as it can prevent over/under-fitting issues. Furthermore, ALLSSA can consider the measurement errors for a more reliable season-trend estimate.

2.2.4. The Auto-Regressive Integrated Moving Average (ARIMA) and Its Extensions

ARIMA is a traditional time series forecasting model based on a time series initial values, lags, and lagged forecast errors [18,19]. If one considers exogenous variables (external data in a forecast), then the model is called ARIMAX [20]. If a time series has seasonal patterns, e.g., climate time series, seasonal terms need to be considered as well; therefore, in this case, the new model is called SARIMAX [21]. The mathematical formulas for ARIMA, ARIMAX, and SARIMAX are given in Equations (1)–(3), respectively.

$$y_t = c + \sum_{n=1}^{p} \alpha_n y_{t-n} + \sum_{n=1}^{q} \theta_n \epsilon_{t-n} + \epsilon_t \tag{1}$$

$$y_t = c + \sum_{n=1}^{p} \alpha_n y_{t-n} + \sum_{n=1}^{q} \theta_n \epsilon_{t-n} + \sum_{n=1}^{r} \beta_n x_{n_t} + \epsilon_t \tag{2}$$

$$y_t = c + \sum_{n=1}^{p} \alpha_n y_{t-n} + \sum_{n=1}^{q} \theta_n \epsilon_{t-n} + \sum_{n=1}^{P} \varphi_n y_{t-sn} + \sum_{n=1}^{Q} \eta_n \epsilon_{t-sn} + \sum_{n=1}^{r} \beta_n x_{n_t} + \epsilon_t \tag{3}$$

where y_t is the lag term; c is the intercept of the models; $\alpha_n, \theta_n, \varphi_n, \eta_n, \beta_n$ are coefficients; p is the trend autoregression order; q is the trend moving average order; P is the seasonal autoregressive order; Q is the seasonal moving average order; r is the number of exogenous variables; s stands for the seasonal effect; ϵ_t is the random error at time t; and x is the exogenous variable. The order of the models plays a crucial role on the result accuracy and could be obtained through a trial-and-error process by minimizing the autocorrelation function and partial autocorrelation function.

3. Results and Discussion

3.1. The MK and Sen's Slope Results

Table 1 lists the Sen's slope results and their MK statistical significance for the Italian regions and for the 12 calendar months. R16, R17, and R19 had significant declining trends in December, while R1 and R2 had significant decreasing trends in September since 2000. In addition, in April, R11, R15, R18, and R19 had significant declining trends since 2000. These results are also in agreement with the monthly gradient estimate maps presented in [12].

Table 1. Sen's slope (mm/year) and its MK significance (* = 90%) (** = 95%) (*** = 99%) for the Italian regions.

R	Jan	Feb	Mar	Apr	May	Jun	Jul	Aug	Sep	Oct	Nov	Dec
1	1.15	0.39	−0.67	−0.19	1.17	0.12	−0.87	−1.03	−2.14 **	0.80	1.75	2.85
2	0.34	−0.19	−0.11	0.48	0.30	0.20	−0.42	−0.76	−2.75 **	0.63	0.80	0.63
3	0.08	−0.22	−0.29	0.05	0.70	1.77	−2.07	−0.16	−1.01	1.72	−2.22	1.75
4	0.89	0.36	−0.95	−0.44	1.09	0.83	−1.56	0.94	0.142	0.68	−2.39	1.14
5	−0.48	1.30	−0.54	−1.34	1.30	0.54	−1.17	0.26	−1.23	0.56	−2.12	0.96
6	0.59	1.89	−1.16	−1.48	2.37	0.94	−1.37	0.46	−0.44	0.17	−1.97	1.34
7	−0.20	0.22	0.16	0.19	−0.35	0.86	0.07	−0.21	−1.08	−0.47	0.60	0.58
8	−0.34	0.92	−0.20	−1.14	0.70	0.50	−0.52	−0.33	−0.81	0.27	−0.29	0.42
9	0.35	1.49	−0.52	−0.91	0.47	0.19	−0.52	−0.25	−0.49	0.46	−0.44	−1.15
10	−0.35	1.17	1.24	−1.16	0.29	1.11	0.15	0.05	−0.04	0.31	0.84	−1.64
11	−0.08	2.06	1.47	−1.98 **	1.12	1.15	0.02	−0.69	−0.83	−0.40	0.24	−2.13
12	−0.75	0.72	0.93	−1.06	−0.03	0.53	0.20	−0.41	0.14	−0.58	0.55	−1.82
13	−0.04	−0.81	1.12	−1.23	−0.10	0.36	0.30	−0.62	−0.86	−0.71	−0.24	−2.89
14	−0.62	−0.31	0.35	−1.32	0.46	0.09	0.64	0.08	0.63	−0.49	2.95	−2.52
15	−0.37	0.22	0.33	−1.41 *	0.59	0.71	−0.02	0.19	0.38	0.52	2.07	−1.41
16	−0.27	0.42	0.50	−1.17	0.39	0.52	0.16	0.38	−0.68	0.42	2.52	−3.11 **
17	0.02	0.00	0.37	−1.60	−0.04	0.75	0.24	0.16	−0.87	0.03	1.96	−3.64 **
18	−0.47	0.27	0.30	−1.86 **	−0.06	0.32	0.44	0.08	−0.87	1.31	2.68	−2.83
19	−2.07	0.47	2.27	−1.98 **	−0.55	−0.32	0.12	0.14	−0.26	1.34	2.66	−4.12 ***
20	−0.23	−0.05	0.62	−1.25	−0.03	0.33	0.01	0.31	1.00	−1.32	0.36	−1.48

3.2. The Boxplots for Monthly Precipitation

The monthly boxplots corresponding to the Italian regions are illustrated in Figure 2. The mean values are shown by ×, while the outliers are shown by °. For example, the outlier observed in the boxplot in Lazio (R12) is for Januar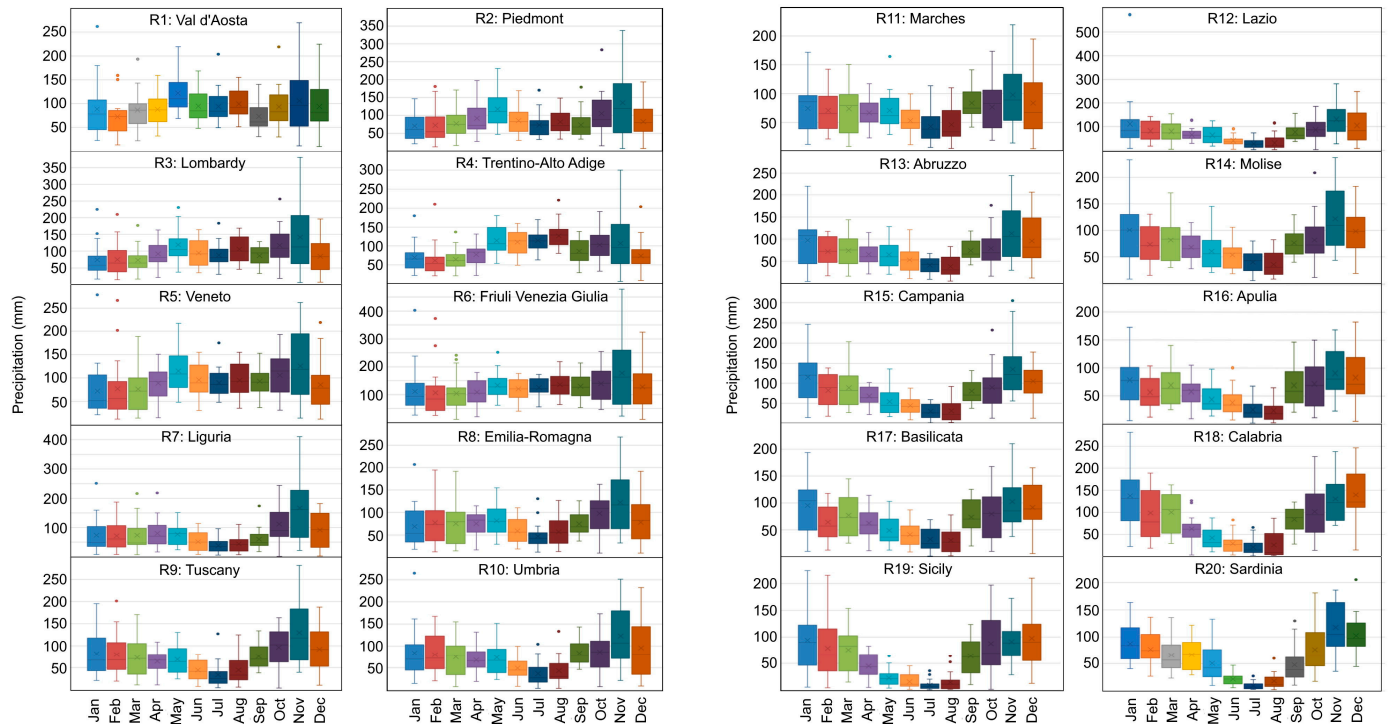y 2021 when Lazio experienced heavy rainfall and flooding: https://world-weather.info/forecast/italy/rome/january-2021 (accessed on 1 January 2023).

Figure 2. The boxplots for GPM monthly precipitation for the Italian regions. The mean is shown by ×, and the outlier is shown by °.

3.3. The ALLSSA Season-Trend Results

The monthly precipitation time series of size 252 corresponding to each Italian region with their simultaneously estimated linear trend and spectral components is illustrated in Figure 3. Except for Val d'Aosta (R1), the other regions had negative precipitation gradients. The monthly precipitation time series for Calabria (R18), Sicily (R19), and Sardinia (R20) had the largest amplitude for their annual cycles (>35 mm) as compared to other regions. Abruzzo (R13) had the most significant declining trend (0.61 mm/year) followed by Lazio (R12) that had a negative rate of 0.43 mm/year since 2000. The high peak observed in R12 in January 2021 and shown as an outlier in the boxplot (see Figure 2) is due to the heavy rainfall/flooding that is likely due to the gradual warming and declining precipitation trend over the past few decades. Note that the extreme values (very high precipitation) generally had higher errors, and therefore, they contributed less to the estimation of the season trend with ALLSSA. The estimated ALLSSA season trend may also be used for forecasting and near-real-time monitoring [22]. Herein, the ALLSSA forecasting performance results were also compared with the auto-regressive moving average-based models.
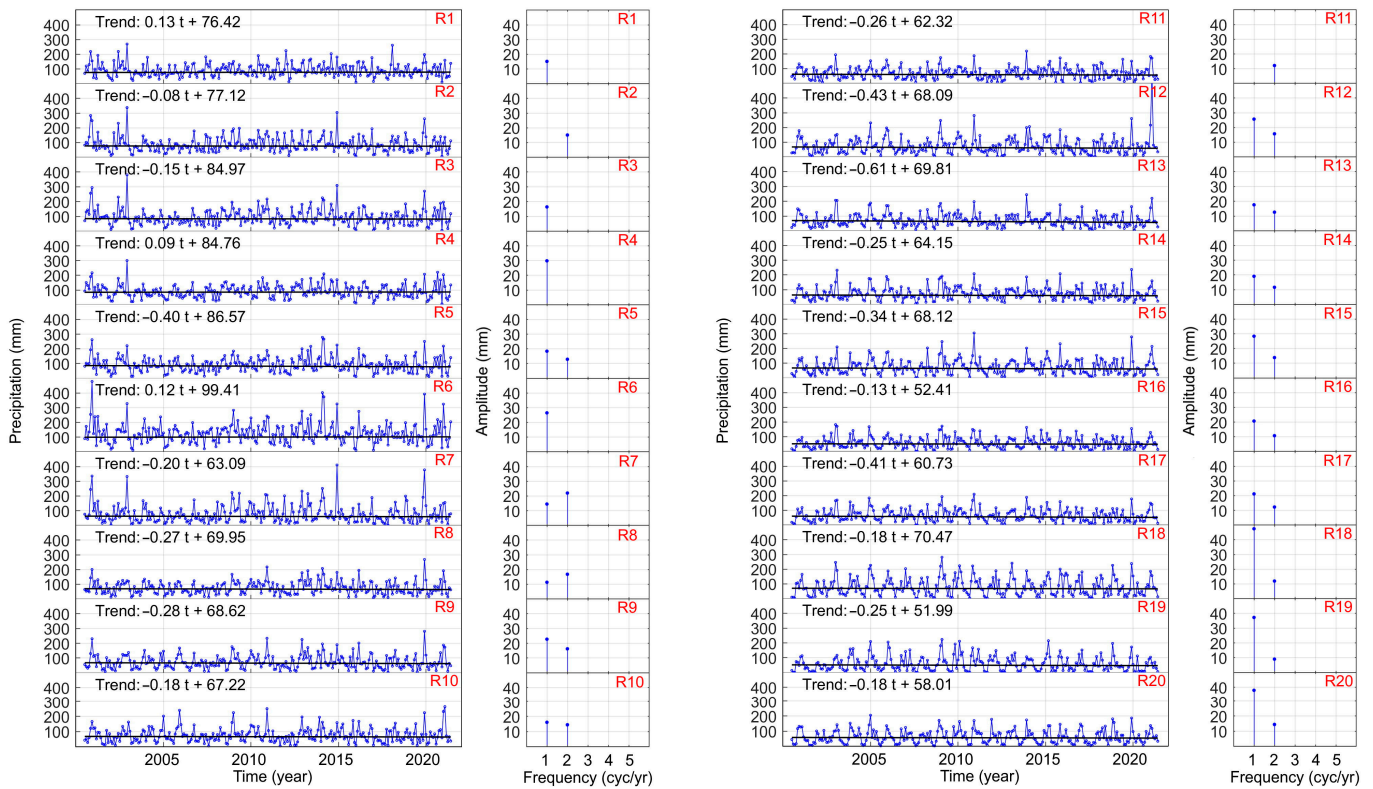
Figure 3. The simultaneous season-trend estimates with ALLSSA at a 99% confidence level. The region IDs shown in red correspond to the ones shown in Figure 1.

3.4. The ARIMA, ARIMAX, SARIMAX, and ALLSSA Results

After converting the time series of each region into a stationary time series by first-order differencing, the most optimized order for each model is proposed, as given in Table 2. The commonly used statistical metrics to evaluate the performance of each model are the mean absolute error (MAE), mean absolute percentage error (MAPE), and root mean square error (RMSE). If y_i and $\hat{y}_i$ are, respectively, the actual and predicted values with n observations, these metrics are mathematically defined by:

$$\text{MAE} = \frac{1}{n}\sum_{i=1}^{n}|\hat{y}_i - y_i| \tag{4}$$

$$\text{MAPE} = 100 \times \frac{1}{n}\sum_{i=1}^{n}\left|\frac{\hat{y}_i - y_i}{y_i}\right| \tag{5}$$

$$\text{RMSE} = \left(\frac{1}{n}\sum_{i=1}^{n}(\hat{y}_i - y_i)^2\right)^{0.5} \tag{6}$$

The values forecasted by the models are compared to the actual values in Figure 4 for Lazio and Calabria. The residual values $\hat{y}_i - y_i$ are also illustrated in Figure 4 for each region. To assess the models' reliability, MAE, MAPE, and RMSE are also calculated for the testing period (June 2020 to June 2021) and shown in Table 2. The period June 2000 to June 2020 was used for training the models (green transparent window in Figure 4), and the period June 2020 to June 2021 was used for testing (yellow transparent window in Figure 4) and forecasting 12 months afterward (blue transparent window in Figure 4).

Table 2. Performance metrics of the forecasting models. ALLSSA outperformed others in terms of MAE, MAPE, and RMSE. Parameters p, d, q are the lag order, the degree of differencing, and the order of moving average, respectively. Parameters P, D, Q, M are the autoregressive order for seasonal component, integration order of the seasonal process, moving average order of the seasonal component, and the number of periods in the season (e.g., 12 for annual data with 12 months in each year), respectively. Note that only the actual and forecasted values in the testing database shown within the yellow transparent window in Figure 4 were used to calculate MAE, MAPE, and RMSE.

	Lazio (R12)				Calabria (R18)			
	ARIMA (p,d,q) (1,1,1)	ARIMAX (p,d,q) (6,1,1)	SARIMAX $(p,d,q)(P,D,Q)[M]$ (3,1,6) (0,1,1) [12]	ALLSSA	ARIMA (p,d,q) (1,1,1)	ARIMAX (p,d,q) (6,1,1)	SARIMAX $(p,d,q)(P,D,Q)[M]$ (3,1,6) (0,1,1) [12]	ALLSSA
MAE (mm)	71.97	72.66	68.54	65.17	43.11	37.15	33.57	23.39
MAPE (%)	84.96	90.97	50.24	42.73	76.32	107.05	61.18	51.34
RMSE (mm)	153.39	153.23	150.25	145.71	57.49	50.20	39.10	27.75

From Figure 4 and the values provided in Table 2, one can observe that ARIMA and ARIMAX have approximately the same results. However, SARIMAX showed more accurate forecasting compared to ARIMA and ARIMAX, which highlights the importance of seasonality effect on the prediction reliability. The comparison between the different techniques is shown in Table 2, and Figure 4 clarifies that, for a time series with a seasonal pattern, SARIMAX can be used, whereas for a non-seasonal time series, both ARIMA or ARIMAX could lead to sufficiently acceptable prediction and forecasting results. For further comparison, ALLSSA was also applied to the monthly precipitation data from June 2000 to June 2020. The ALLSSA-estimated coefficients of harmonics and trend were used to forecast the monthly precipitation for June 2020 to June 2021. Using the actual measurements for June 2020 to June 2021, the statistical metrics were then calculated. From Table 2 obtained on the testing period, one can observe that ALLSSA outperformed ARIMA, ARIMAX, and SARIMAX for forecasting.

From the residual panel in Figure 4, all the models performed poorly for predicting the precipitation in January 2021 in Lazio. In fact, extreme precipitation events cannot be well predicted due to their abrupt behavior (e.g., precipitation value in January 2021 detected as an outlier in Figure 2). Figure 3 shows that Lazio historically had heavy precipitation in the months of November to February (e.g., November 2010 and 2019, December 2005 and 2009, January 2014 and 2021) when most of the destructive landslides occurred [7,8]. Due to factors such as gradual warming, declining annual precipitation, and changes in land cover [12], it is expected that the frequency of heavy rainfall in Lazio and other similar regions will increase in the upcoming years, posing a great risk for more landslides to occur. This also highlights the importance of conducting this research.

There are several other time series analysis methods for prediction and forecasting. For example, Song and Chissom [23] describe fuzzy time series and develop fuzzy time series models. The fundamental concept of this forecasting approach is replacing real values with fuzzy sets and could be performed through four main steps: (i) defining the universe of discourse and splitting it into intervals; (ii) determining the fuzzy sets on the universe of discourse and fuzzifying the time series; (iii) developing the model of the existing fuzzy-logic relationships in the fuzzified time series; and (iv) forecasting and eventually de-fuzzifying the forecasted values [24]. Novak et al. applied the fuzzy transform theory for time series analysis and forecasting for the first time [25]. Implementing such fuzzy models for processing precipitation time series could also be interesting and is subject to future studies.
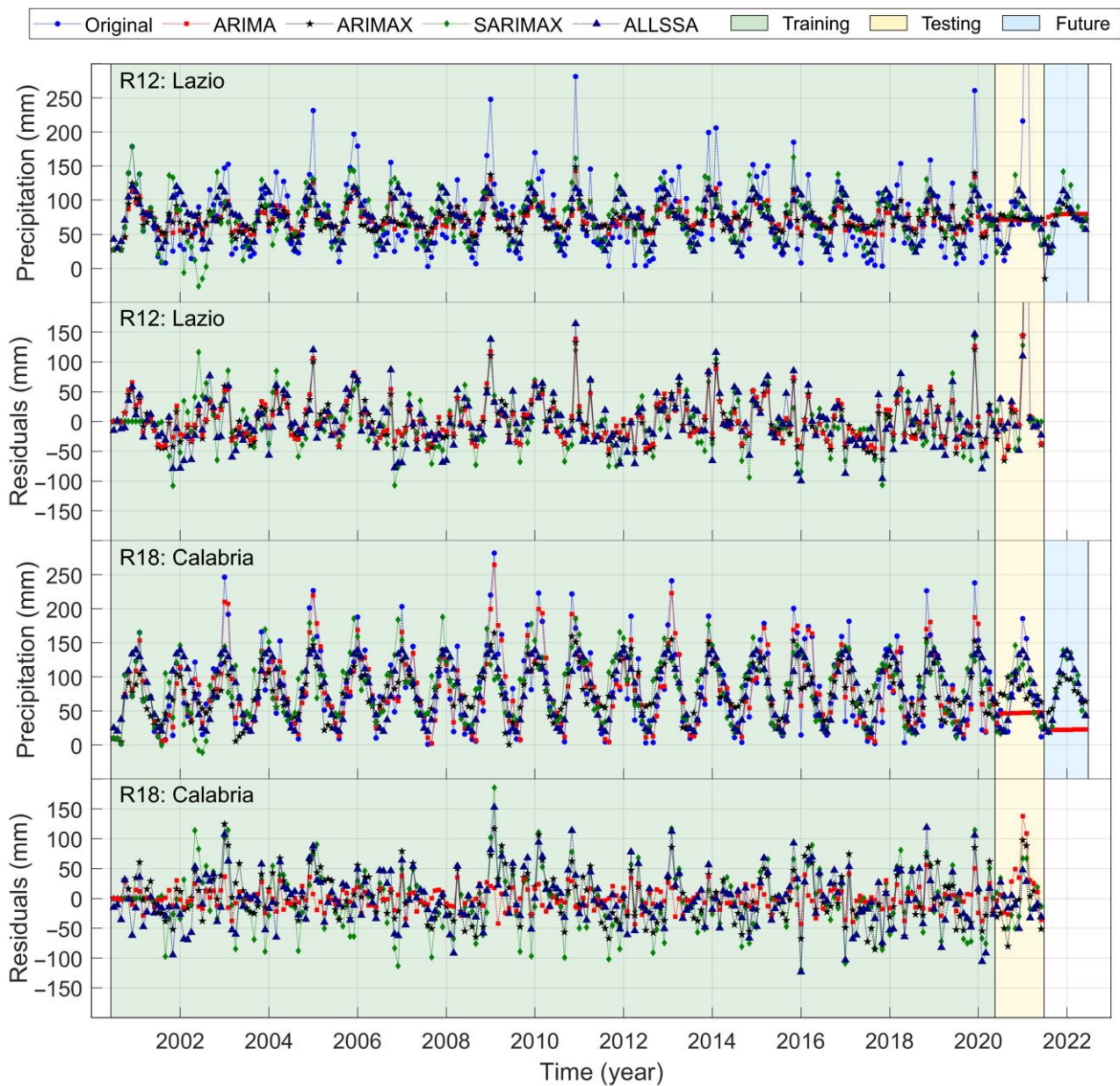
Figure 4. Comparison between the actual values and the predicted values with the ARIMA, ARIMAX, SARIMAX, and ALLSSA models for Lazio (R12) and Calabria (R18). The residual series are obtained by subtracting the predicted values from the actual values.

4. Conclusions

In this paper, we estimated the trend and seasonal components of the monthly precipitation time series for the twenty administrative regions of Italy. Using the Mann–Kendall test, we found that April, September, and December were the only months when precipitation had a declining trend at a 95% confidence level for northern and southern regions. The ALLSSA also showed negative declining trends for all the regions except Val d'Aosta, and annual cycles were most pronounced in the southern part of Italy: Calabria, Sicily, and Sardinia. We also compared the forecasting performances of ARIMA, ARIMAX, SARIMAX, and ALLSSA for Lazio that had extreme precipitation events during winter and Calabria that had the most significant seasonality. We found that ALLSSA had a better performance than ARIMA, ARIMAX, and SARIMAX for prediction and forecasting. However, all the models performed poorly for predicting extreme precipitation. Hybrid models that consider other parameters, such as temperature, soil moisture, and wind, may produce

better and more reliable forecasting results. We hope our findings can help policymakers and stakeholders develop proper risk management strategies to maintain a sustainable environment.

References

1. Gentilucci, M.; Materazzi, M.; Pambianchi, G. Statistical Analysis of Landslide Susceptibility, Macerata Province (Central Italy). *Hydrology* **2021**, *8*, 5. [CrossRef]
2. Mazzanti, P.; Bozzano, F.; Cipriani, I.; Prestininzi, A. New insights into the temporal prediction of landslides by a terrestrial SAR interferometry monitoring case study. *Landslides* **2015**, *12*, 55–68. [CrossRef]
3. Koehler, J.; Dietz, A.J.; Zellner, P.; Baumhoer, C.A.; Dirscherl, M.; Cattani, L.; Vlahović, Ž.; Alasawedah, M.H.; Mayer, K.; Haslinger, K.; et al. Drought in Northern Italy: Long Earth Observation Time Series Reveal Snow Line Elevation to Be Several Hundred Meters Above Long-Term Average in 2022. *Remote Sens.* **2022**, *14*, 6091. [CrossRef]
4. Malandra, F.; Vitali, A.; Morresi, D.; Garbarino, M.; Foster, D.E.; Stephens, S.L.; Urbinati, C. Burn Severity Drivers in Italian Large Wildfires. *Fire* **2022**, *5*, 180. [CrossRef]
5. Marino, D.; Palmieri, M.; Marucci, A.; Soraci, M.; Barone, A.; Pili, S. Linking Flood Risk Mitigation and Food Security: An Analysis of Land-Use Change in the Metropolitan Area of Rome. *Land* **2023**, *12*, 366. [CrossRef]
6. Marchesini, I.; Ardizzone, F.; Alvioli, M.; Rossi, M.; Guzzetti, F. Non-susceptible landslide areas in Italy and in the Mediterranean region. *Nat. Hazards Earth Syst. Sci.* **2014**, *12*, 2215–2231. [CrossRef]
7. Lombardi, A.; Gallicchio, D.; Tomassetti, B.; Raparelli, E.; Tuccella, P.; Lidori, R.; Verdecchia, M.; Colaiuda, V. Evaluating the Response of Hydrological Stress Indices Using the CHyM Model over a Wide Area in Central Italy. *Hydrology* **2022**, *9*, 139. [CrossRef]
8. Alessi, D.; Bozzano, F.; Di Lisa, A.; Esposito, C.; Fantini, A.; Loffredo, A.; Martino, S.; Mele, F.; Moretto, S.; Noviello, A.; et al. Geological risks in large cities: The landslides triggered in the city of Rome (Italy) by the rainfall of 31 January–2 February 2014. *Ital. J. Eng. Geol. Environ.* **2014**, *1*, 15–34.
9. Shawky, M.; Moussa, A.; Hassan, Q.K.; El-Sheimy, N. Performance Assessment of Sub-Daily and Daily Precipitation Estimates Derived from GPM and GSMaP Products over an Arid Environment. *Remote Sens.* **2019**, *11*, 2840. [CrossRef]
10. Huffman, G.J.; Stocker, E.F.; Bolvin, D.T.; Nelkin, E.J.; Tan, J. GPM IMERG Final Precipitation L3 1 month 0.1 degree x 0.1 degree V06 (GPM_3IMERGM). 2019. [CrossRef]
11. Pradhan, R.K.; Markonis, Y.; Godoy, M.R.V.; Villalba-Pradas, A.; Andreadis, K.M.; Nikolopoulos, E.I.; Papalexiou, S.M.; Rahim, A.; Tapiador, F.J.; Hanel, M. Review of GPM IMERG performance: A global perspective. *Remote Sens. Environ.* **2022**, *268*, 112754. [CrossRef]
12. Ghaderpour, E.; Mazzanti, P.; Scarascia Mugnozza, G.; Bozzano, F. Coherency and phase delay analyses between land cover and climate across Italy via the least-squares wavelet software. *Int. J. Appl. Earth Obs. Geoinf.* **2023**, *118*, 103241. [CrossRef]
13. Shawky, M.; Ahmed, M.R.; Ghaderpour, E.; Gupta, A.; Dewan, A.; Hassan, Q.K. Remote sensing-derived land surface temperature trends over South Asia. *Ecol. Inform.* **2023**, *74*, 101969. [CrossRef]
14. Zaghloul, M.S.; Ghaderpour, E.; Dastour, H.; Farjad, B.; Gupta, A.; Eum, H.; Achari, G.; Hassan, Q.K. Long Term Trend Analysis of River Flow and Climate in Northern Canada. *Hydrology* **2022**, *9*, 197. [CrossRef]

15. McGill, R.; Tukey, J.; Larsen, W. Variations of box plots. *Am. Stat.* **1978**, *32*, 12–16.
16. Ghaderpour, E. JUST: MATLAB and Python software for change detection and time series analysis. *GPS Solut.* **2021**, *25*, 85. [CrossRef]
17. Ghaderpour, E.; Vujadinovic, T.; Hassan, Q.A. Application of the Least-Squares Wavelet software in hydrology: Athabasca River Basin. *J. Hydrol. Reg. Stud.* **2021**, *36*, 100847. [CrossRef]
18. McKenzie, E.D. General exponential smoothing and the equivalent ARMA process. *J. Forecast.* **1984**, *3*, 333–344. [CrossRef]
19. Barba, P.; Rosado, B.; Ramírez-Zelaya, J.; Berrocoso, M. Comparative Analysis of Statistical and Analytical Techniques for the Study of GNSS Geodetic Time Series. *Eng. Proc.* **2021**, *5*, 21.
20. Jalalkamali, A.; Moradi, M.; Moradi, N. Application of several artificial intelligence models and ARIMAX model for forecasting drought using the Standardized Precipitation Index. *Int. J. Environ. Sci. Technol.* **2015**, *12*, 1201–1210. [CrossRef]
21. Manigandan, P.; Alam, M.S.; Alharthi, M.; Khan, U.; Alagirisamy, K.; Pachiyappan, D.; Rehman, A. Forecasting Natural Gas Production and Consumption in United States-Evidence from SARIMA and SARIMAX Models. *Energies* **2021**, *14*, 6021. [CrossRef]
22. Ghaderpour, E.; Vujadinovic, T. The Potential of the Least-Squares Spectral and Cross-Wavelet Analyses for Near-Real-Time Disturbance Detection within Unequally Spaced Satellite Image Time Series. *Remote Sens.* **2020**, *12*, 2446. [CrossRef]
23. Song, Q.; Chissom, B.S. Fuzzy time series and its models. *Fuzzy Sets Syst.* **1993**, *54*, 269–277. [CrossRef]
24. Zhang, Y.; Qu, H.; Wang, W.; Zhao, J. A novel fuzzy time series forecasting model based on multiple linear regression and time series clustering. *Math. Probl. Eng.* **2020**, *2020*, 9546792. [CrossRef]
25. Novák, V.; Perfilieva, I.; Dvorak, A. *Insight into Fuzzy Modeling*; John Wiley & Sons: Hoboken, NJ, USA, 2016.